# Resistive-Sensor Interfacing Circuit for Remote Measurement Using CFOA

Wandee Petchmaneelumka[1], Apinai Rerkratn[1,*], Sirichai Tammaruckwattana[1], and Anucha Kaewpoonsuk[2]
[1] School of Engineering, King Mongkut's Institute of Technology Ladkrabang, Bangkok, Thailand
[2] Faculty of Science, Naresuan University, Phitsanulok, Thailand
Email: wandee.pe@kmitl.ac.th (W.P.), apinai.re@kmitl.ac.th (A.R.), sirichai.ta@kmitl.ac.th (S.T.), anuchak@nu.ac.th (A.K.)

***Abstract*—An alternative approach to implementing an interfacing circuit for resistive sensor-based remote measurement is presented. The proposed technique uses a Current Feedback Operational Amplifier (CFOA) as an active building block to produce an output voltage linearly related to the resistance of the sensor. Moreover, the accuracy of the output voltage is improved by the enhancement of CFOA. In addition, the proposed circuit provides compensation for the effects of lead-wire resistance. The performance of the proposed technique is discussed in detail and confirmed by PSPICE program simulation and experimental implementation. The resistance decade box is used in the experiment. The maximum error on the output voltage of the experimental results is about 0.4234 %. The experimental results show that the proposed technique provides good performance.**

***Index Terms*—interfacing circuit, resistive sensor, remote measurement, Current Feedback Operational Amplifier (CFOA)**

## I. Introduction

A resistive sensor is a transducer device that converts changes in a specific physical quantity into an electrical signal that can be observed after signal conditioning. Physical quantities can be measured using resistance change such as temperature (resistance temperature detector: RTD, and thermistors), light (light-dependent resistor), mechanical deformation (piezo-resistive sensor), and magnetic field strength (magneto resistive sensor) [1–3]. By special structure design and construction or material variety, resistive sensors can be useful for detecting other physical quantities such as force and torque, distance and angle, pressure, acceleration, velocity, and so on. Due to the simplicity of their working principle, these sensors are used in many applications such as consumer electronics [4–6], wearable human-machine interfaces [7–9], medical equipment and instruments [10], industrial measurement and instruments [11, 12], etc. The main benefits of resistive sensors are small size, ease of integration, simple readout electronics, flexibility, and low cost [1–3]. There are many techniques for converting the resistance of the resistive sensor. The output characteristics of the interface circuit for resistive sensors can be separated into 2 main types, analog and digital schemes. For the analog scheme, the DC voltage output is relative to the resistance of the resistive sensor, while the digital scheme, the frequency or period of voltage output is relative to the resistance of the resistive sensor. There are many techniques for analog interfacing with the resistive sensor. The technique of converting the resistance of the resistive sensor to analog output without compensating for lead wire resistance has been proposed [13, 14]. To improve the mentioned technique, the methods to convert the resistance of the resistive sensor to analog output with compensation of lead wire resistance using diodes [15, 16], Zener diode [17], and without diode [18] have been presented. The digital interface method is a widely technique for converting the resistive sensor. The circuit techniques for converting the resistance of the resistive sensor to digital output based on a relaxation oscillator [19, 20], and operational amplifiers [21, 22], without compensating for lead wire resistance have been proposed. To compensate for the lead wire resistance, the interfacing circuit techniques for converting the resistance of the resistive sensor to digital output using operational amplifiers with diodes [23, 24], operational amplifiers without diode [25–27], and microcontroller [28–30] have been presented. For industrial applications, resistive sensors are widely used in measurement, instrumentation, control, and monitoring systems. Unfortunately, for safety reasons, sensors are located separately from measurement systems which contain signal conditioners and signal processing systems. Resistance of lead-wire connecting between the sensors and measurement systems increases directly proportional to the lead-wire length. This resistance causes errors in the output of the measurement systems.

The compensation technique for lead wire resistance utilizing the properties of the diode to control the direction of the current flowing through a resistive sensor is one of the interesting techniques for simple interface circuit design. Based on the above technique, the approach using a clock generator circuit, constant current source, switching network, sample and hold circuit, and two diodes has been introduced [31]. The approach based on the V-to-I converter consisting of two op-amps connected with two diodes to compensate for the lead wire resistance has been presented [32]. Another approach based on the use of the second-generation current conveyor operational amplifier

Manuscript received March 14, 2024; revised May 13, 2024; accepted May 20, 2024.
*Corresponding author.

(CCII), sample and hold (S/H), and two diodes to compensate for the effect of the lead-wire resistance has been proposed [33]. Moreover, the mentioned compensation techniques based on a microcontroller and operational amplifier connected with two diodes to compensate for the lead-wire resistance have been presented [15, 16].

This paper proposes a simple and low-cost interfacing circuit for a resistive sensor with lead-wire-resistance compensation. The technique to compensate for lead-wire resistance is based on diode properties to control the current flowing direction through a resistive sensor. The proposed interfacing circuit provides the analog output. The measured resistance of the resistive sensors in the form of the voltage output corresponds to the sensor's resistance. In addition, the lead wire resistance effect causing the output signal error is compensated. The realization method based on two diodes is the same as in [15, 16], but the difference is that the design uses only one Current Feedback Operational Amplifier (CFOA). The proposed method provides a simple circuit without the requirement of an analog switch, resulting in a smaller and more economical circuit. The performance of the proposed circuit is confirmed through a simulation program and experiment with commercially available devices.

## II. Circuit Descriptions

### A. The Proposed Interface Circuit

The proposed block diagram of the interface circuit for resistive sensor-based remote measurement using a CFOA with lead-wire-resistance compensation is shown in Fig. 1.

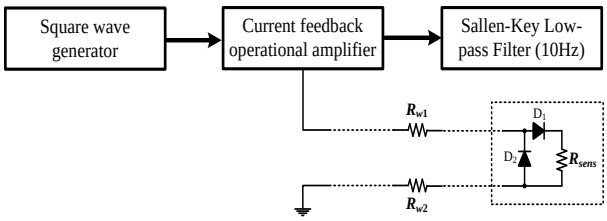


Fig. 1. Block diagram of the interface circuit for resistive sensor-based remote measurement using a CFOA.

The block diagram in Fig. 1 consists of a square wave generator, a current feedback operational amplifier (CFOA), a sallen-key low-pass filter with 10Hz cut-off frequency, commercially available diodes, and the sensing resistor ($R_{sens}$).

### B. Signal Generator

The signal generator is an electronic device that creates signals such as sine, square, triangular, and saw-tooth waves. Sine and square wave signals are most used in electronic instrument systems, test and measurement systems, and modern communication systems [33–35]. Voltage-Controlled Oscillators (VCOs) are commonly used to create sine and square waves. Many approaches propose voltage-controlled oscillators with low noise and low power consumption for application in mobile devices [34, 35]. This article uses an RC relaxation oscillator generating a square wave signal for controlling CFOA. A sine wave signal can be used to control CFOA; however, a square wave signal makes it easier to control the amplitude.

### C. Current Feedback Operational Amplifier

The key part of the proposed interfacing circuit is CFOA. It is based on AD844, which consists of a second-generation current conveyor (CCII) connected with a voltage follower circuit as shown in Fig. 2(a). The symbol of CFOA is demonstrated in Fig. 2(b). Ideally, CCII provides the following relationships:

$$I_y = 0, V_x = V_y, I_z = I_x, V_w = V_z, \quad (1)$$

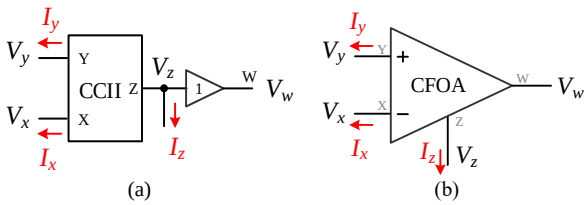


Fig. 2. Current Feedback Operational Amplifier: (a) The structure of the CFOA and (b) CFOA symbol.

### D. The Proposed Sensing Circuit

The proposed sensing circuit is shown in Fig. 3, where $R_{sens}$ and ($R_{w1}$ and $R_{w2}$) represent the resistance of the sensor and the first and second lead-wire resistances connected between the sensor and the measurement circuit, respectively.

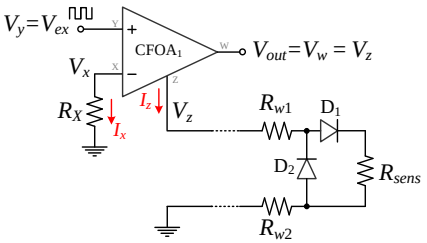


Fig. 3. The proposed sensing circuit.

From the interface circuit in Fig. 3, the square wave signal ($V_{ex}$) is applied to port Y of CFOA to produce voltage and current of CFOA with values as follows:

$$V_x = V_y = V_{ex} \quad (2)$$

$$I_z = I_x = \frac{V_{ex}}{R_X} \quad (3)$$

From Fig. 3 when the square wave signal $V_{ex}$ is a positive pulse, the current $I_z$ flows out from port Z through lead wire $R_{w1}$, diode $D_1$, $R_{sens}$, and lead wire $R_{w2}$. The voltage $V_z$ can be written as

$$V_z = (R_{sens} + R_{w1} + R_{w2})I_z + V_{D1} \quad (4)$$

where $V_{D1}$ is the voltage drop across the diode $D_1$.

When the square wave signal $V_{ex}$ is a negative pulse, the current $I_z$ flows in port Z through lead wire $R_{w2}$, diode $D_2$, $R_{sens}$, and lead wire $R_{w1}$. The voltage $V_z$ can be stated as

$$V_z = (R_{w1} + R_{w2})I_z + V_{D2} \quad (5)$$

where $V_{D2}$ is the voltage drop across the diode $D_2$.

From (3) to (5), the voltage $V_z$ alternates positive pulse and negative pulse. Thus, the output voltage of CFOA ($V_w$) corresponds to the voltage $V_z$ as

$$V_{w+} = V_z = (R_{sens} + R_{w1} + R_{w2})\frac{V_{ex}}{R_X} + V_{D1} \quad (6)$$

$$V_{w-} = V_z = -\left[(R_{w1} + R_{w2})\frac{V_{ex}}{R_X} + V_{D2}\right] \quad (7)$$

And then the average output voltage of the proposed interfacing circuit ($V_{out}$) can be written as

$$V_{out} = 0.5\left(R_{sens}\frac{V_{ex}}{R_X} + V_{D1} - V_{D2}\right) \quad (8)$$

From (8), if diodes $D_1$ and $D_2$ are matched, then the average output of this circuit can be rewritten as

$$V_{out} = 0.5R_{sens}\frac{V_{ex}}{R_X} \quad (9)$$

If the parameters $V_{ex}$ and $R_X$ in (9) are the constant values, the amplitude of signal $V_{out}$ is directly proportional to the sensing resistance $R_{sens}$.

From (9), the accuracy of the output voltage of the proposed interfacing circuit depends on the accuracy of CFOA. The method to improve the accuracy of CFOA is to place the opamp with negative feedback connection to the input of CFOA for reduction of the effect of the internal resistance of port X [36, 37]. The improved circuit diagram of the proposed interfacing circuit for resistive sensor-based remote measurement using a CFOA can be demonstrated in Fig. 4.

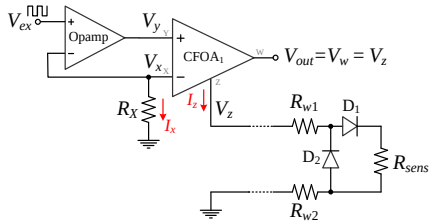


Fig. 4. The improved circuit diagram of the proposed simple interfacing circuit.

## III. Simulation Studies

The proposed interface circuits for the resistive sensor in Fig. 3 and Fig. 4 were simulated using ORCAD PSPICE Release 9.2 to verify the functionality and efficiency of each circuit. The parameter of simulation values of the electronic components used were set as $R_X$ = 5 kΩ, $D_1$ and $D_2$ are general purpose diodes 1N4148. The models of active devices CFOA and op-amp used for simulation are AD844 and LF351, respectively. The signal $V_{ex}$ was set to 10 Vp-p with frequency 1 kHz and 50% duty-cycle. The power supply voltages were set to ±12 V. For remote measurement simulation, the lead-wire resistances ($R_{w1}$ and $R_{w2}$) and the sensing resistance $R_{sens}$ were set at different values. The lead-wire resistances $R_{w1}$ and $R_{w2}$ are varied with 5 cases as Case 1: $R_{w1} = R_{w2} = 0$ Ω, Case 2: $R_{w1} = R_{w2} = 25$ Ω, Case 3: $R_{w1} = R_{w2} = 50$ Ω, Case 4: $R_{w1} = R_{w2} = 75$ Ω, and Case 5: $R_{w1} = R_{w2} = 100$ Ω.

The sensing resistors $R_{sens}$ was varied in the range of 0.5 kΩ to 1.5 kΩ. The simulation results for 5 cases of the proposed circuits in Fig. 3 and Fig. 4 are shown in Table I and Table II, respectively. The worst-case error of the results in Table I and Table II are about –0.90693% and –0.0561%, respectively.

TABLE I: SIMULATION RESULTS OF THE PROPOSED CIRCUIT OF FIG. 3 FOR DIFFERENTIAL VALUES OF LEAD RESISTANCES

| $R_{sens}$ (Ω) | Calculated $V_o$ (mV) | Measured $V_o$ (mV) | | | | | Worst-case error (%) |
|---|---|---|---|---|---|---|---|
| | | Case 1 | Case 2 | Case 3 | Case 4 | Case 5 | |
| 500 | 250.00 | 247.84 | 247.84 | 247.80 | 247.80 | 247.80 | −0.8816 |
| 600 | 300.00 | 297.39 | 297.39 | 297.40 | 297.35 | 297.35 | −0.88383 |
| 700 | 350.00 | 346.99 | 346.94 | 346.95 | 346.90 | 346.90 | −0.88614 |
| 800 | 400.00 | 396.54 | 396.49 | 396.50 | 396.45 | 396.45 | −0.88787 |
| 900 | 450.00 | 446.09 | 446.04 | 446.05 | 446.00 | 446.00 | −0.88922 |
| 1000 | 500.00 | 495.64 | 495.59 | 495.60 | 495.55 | 495.50 | −0.8997 |
| 1100 | 550.00 | 545.19 | 545.14 | 545.10 | 545.10 | 545.05 | −0.89973 |
| 1200 | 600.00 | 594.74 | 594.69 | 594.64 | 594.65 | 594.60 | −0.89975 |
| 1300 | 650.00 | 644.24 | 644.24 | 644.20 | 644.15 | 644.15 | −0.90023 |
| 1400 | 700.00 | 693.79 | 693.74 | 693.75 | 693.70 | 693.65 | −0.90693 |
| 1500 | 750.00 | 743.34 | 743.29 | 743.25 | 743.20 | 743.20 | −0.90687 |

TABLE II: SIMULATION RESULTS OF THE PROPOSED CIRCUIT OF FIG. 4 FOR DIFFERENTIAL VALUES OF LEAD RESISTANCES

| $R_{sens}$ (Ω) | Calculated $V_o$ (mV) | Measured $V_o$ (mV) | | | | | Worst-case error (%) |
|---|---|---|---|---|---|---|---|
| | | Case 1 | Case 2 | Case 3 | Case 4 | Case 5 | |
| 500 | 250.00 | 249.99 | 249.99 | 250.03 | 250.07 | 250.07 | 0.0296 |
| 600 | 300.00 | 299.94 | 299.99 | 299.98 | 300.02 | 300.07 | 0.0233 |
| 700 | 350.00 | 349.89 | 349.93 | 349.98 | 350.02 | 350.02 | −0.0320 |
| 800 | 400.00 | 399.89 | 399.89 | 399.93 | 399.97 | 399.97 | −0.0288 |
| 900 | 450.00 | 449.84 | 449.89 | 449.88 | 449.92 | 449.97 | −0.0353 |
| 1000 | 500.00 | 499.79 | 499.83 | 499.88 | 499.87 | 499.92 | −0.0417 |
| 1100 | 550.00 | 549.79 | 549.78 | 549.83 | 549.82 | 549.87 | −0.0393 |
| 1200 | 600.00 | 599.74 | 599.74 | 599.78 | 599.77 | 599.82 | −0.0442 |
| 1300 | 650.00 | 649.69 | 649.69 | 649.73 | 649.72 | 649.77 | −0.0485 |
| 1400 | 700.00 | 699.64 | 699.64 | 699.68 | 699.67 | 699.67 | −0.0521 |
| 1500 | 750.00 | 749.59 | 749.58 | 749.58 | 749.62 | 749.62 | −0.0561 |

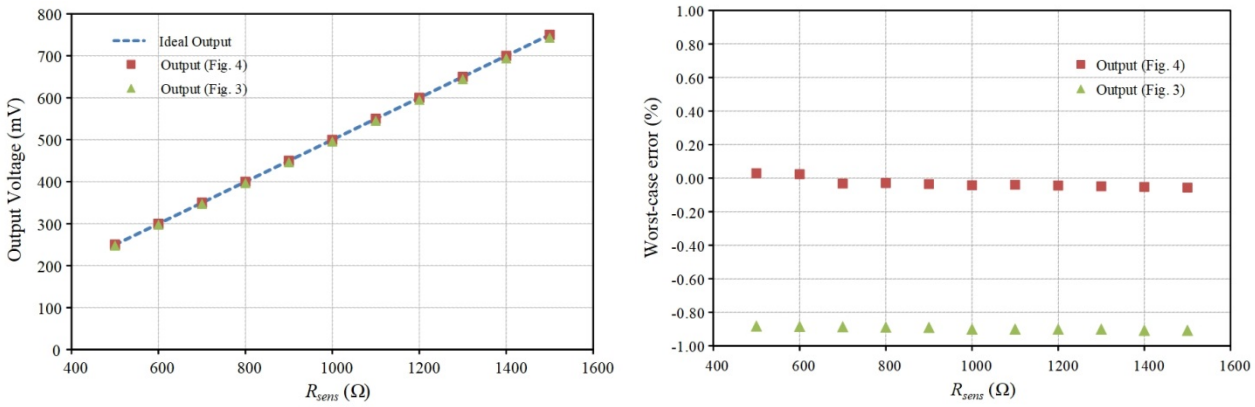


(a) (b)

Fig. 5. The performance of the improved circuit: (a) The plots of the simulated output voltage ($V_{out}$) against the sensing resistors ($R_{sens}$) for Case 1 and (b) The worst-case error of the proposed circuit for the sensing resistors $R_{sens}$ in the range of 0.5 kΩ to 1.5 kΩ.

The results for case 1 in Table I and Table II are plotted to confirm the performance of the improved circuit in Fig. 4, as shown in Fig. 5.

Fig. 5(a) shows the plots of the simulated output voltage ($V_{out}$) against the sensing resistance ($R_{sens}$) varied in the range of 0.5 kΩ to 1.5 kΩ for case 1. This figure shows that the improved circuit can reduce the effect of the internal resistance of port X. Fig. 5(b) demonstrates the comparison of worst-case error between the sensing circuit and the improved sensing circuit for the sensing resistance $R_{sens}$ varied in the range of 0.5 kΩ to 1.5 kΩ of 5 cases. From the results in Table I and Table II, it can be seen that the improved circuit can reduce the error of the output voltage of the proposed circuit. The simulated results show that the improved circuit diagram of the proposed simple interfacing circuit is suitable for interfacing with resistive sensor-based remote measurement. This circuit will be used in a practical experiment to test the performance of the proposed circuit.

## IV. Experimental Setup

From Fig. 4, the improved circuit diagram of the proposed simple interfacing circuit is used for the experiment. The square wave generator is used to generate the signal ($V_{ex}$) shown in Fig. 6.

From Fig. 6, the square wave generator is an astable oscillator circuit that generates a rectangular output waveform using an RC network. The oscillation frequency of the circuit depends on the charge and discharge of the capacitor $C_1$ through the feedback resistor $R_1$. The square wave generator is set to generate the output signal ($V_{ex}$) with 1 kHz of frequency and a 50 % duty cycle. The Zener diodes $Z_1$ and $Z_2$ are used to maintain the output voltage of the square wave generator circuit to 13.8 Vp-p. Sallen-key low-pass filter with a 10 Hz cut-off frequency is used to approximate the average value of $V_w$ in Fig. 4, as shown in Fig. 7. The variable resistor ($VR_2$) is used to adjust the voltage gain of the low-pass filter to 2. From the circuits in Fig. 4, Fig. 6, and Fig. 7, the proposed circuit diagram of the interface circuit for a resistive sensor with lead wire compensation can be shown in Fig. 8. The circuit in Fig. 8 was experimentally implemented using commercial AD844, LF351, 1N4148, and 1N4735 for CFOA, op-amp, diodes, and Zener diodes, respectively. The values of the electronic components used were set as $R_1$=$R_7$ =50 kΩ, $R_2$=1 kΩ, $R_3$=$R_4$ =$R_8$=10 kΩ, $R_5$=3.3 kΩ, $R_6$=20 kΩ, $VR_1$=$VR_2$=100 kΩ, $VR_X$=10 kΩ, $C_1$=1 nF, $C_2$=$C_3$=0.47 μF while all devices are powered by ±12 V power supply. From the given parameter, the proposed circuit can measure the resistance of a resistive sensor in the range of 0–10 kΩ.

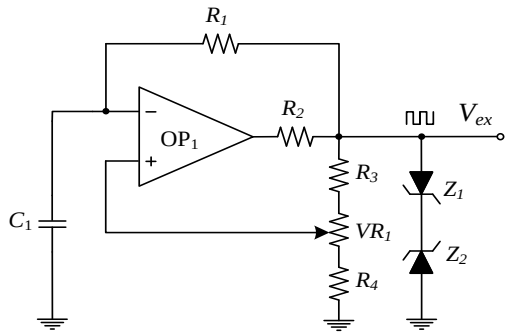


Fig. 6. The simple square wave generator for use in the proposed interfacing circuit.

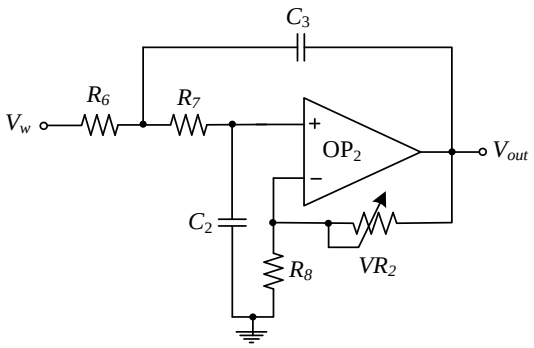


Fig. 7. Sallen-key low-pass filter with 10 Hz cut-off frequency.

For the experimental remote measurement, the lead-wire resistances ($R_{w1}$ and $R_{w2}$) and the sensing resistance $R_{sens}$ were set at different values. The lead-wire resistances $R_{w1}$ and $R_{w2}$ are varied in 5 cases as Case 1: $R_{w1}$=$R_{w2}$=0 Ω, Case 2: $R_{w1}$=$R_{w2}$ = 25 Ω, Case 3: $R_{w1}$=$R_{w2}$ =50 Ω, Case 4: $R_{w1}$=$R_{w2}$=75 Ω, and Case 5: $R_{w1}$=$R_{w2}$=100 Ω. The sensing resistors $R_{sens}$ was varied in the range of 0.5 kΩ to1.5 kΩ.

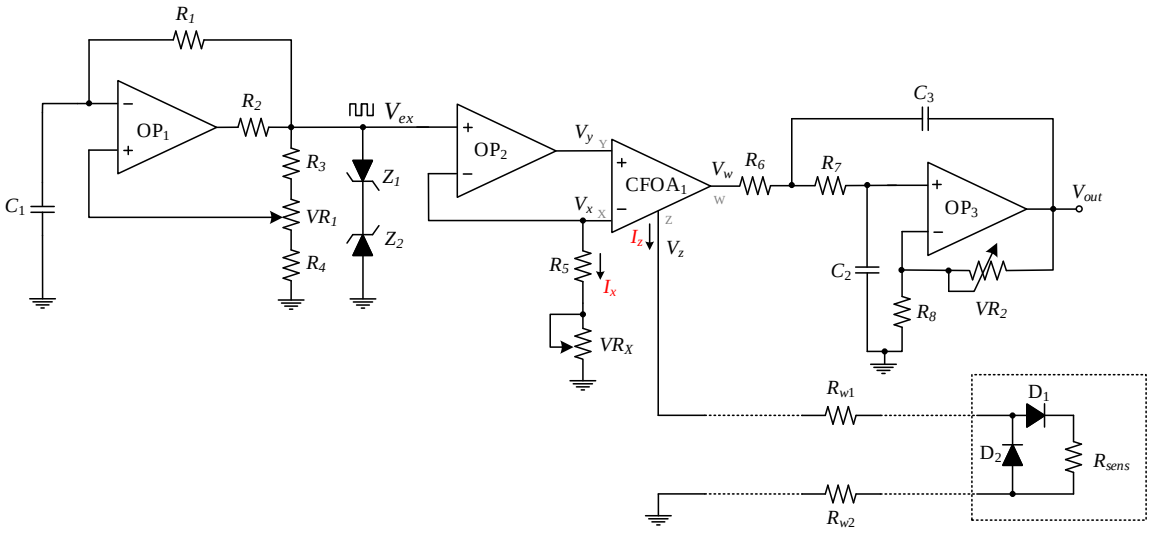


Fig. 8. The circuit diagram of the proposed interface circuit.

## V. Experimental Results

Fig. 9 shows the measured signal of the square wave generator circuit. This figure demonstrates the square wave signal with an amplitude of about 13.8 Vp-p and 50% duty cycle. The signal from the square wave generator is sent to CFOA via opamp $OP_1$ to generate the current $I_z$. The variable resistor ($VR_1$) is used to adjust the frequency of the square wave generator to 1 kHz. The variable resistor ($VR_X$) is used to vary the magnitude of the current $I_z$ to 2 mAp-p before it is sent to sensing resistors $R_{sens}$. Fig. 10 shows the measured signal of the sensing circuit in case 1 with $R_{sens}$ set to 1 kΩ. The signal in trace 1 shows the input signal of opamp $OP_2$ while the signal in trace 2 shows the output signal of CFOA. Fig. 11 demonstrates the measured signal of the low-pass filter circuit in case 1 with $R_{sens}$ set to 1 kΩ. The signal in trace 1 shows the input signal low pass filter circuit while the signal in trace 2 shows the output signal of the proposed circuit. The DC output voltage of the low-pass filter corresponds to the sensing resistance $R_{sens}$.

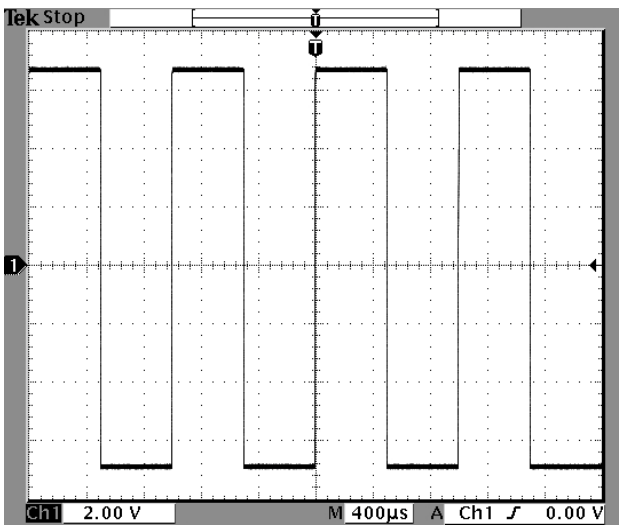


Fig. 9. Measured signal of the square wave generator circuit.

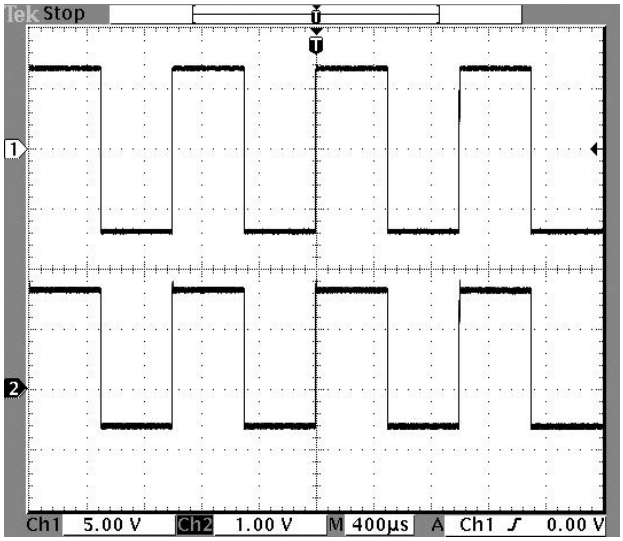


Fig. 10. Measured signal of the sensing circuit in case 1 with $R_{sens}$ set to 1 kΩ. Trace 1: input signal, Trace 2: output signal.

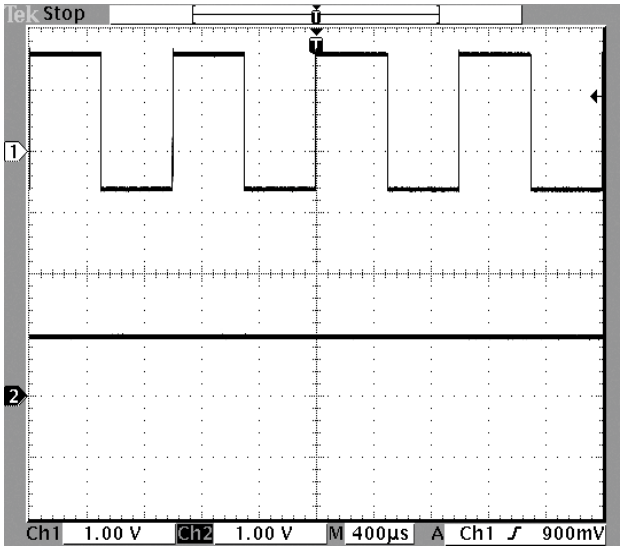


Fig. 11. Measured signal of low-pass filter circuit in case 1 with $R_{sens}$ set to 1 kΩ. Trace 1: input signal, Trace 2: output signal.

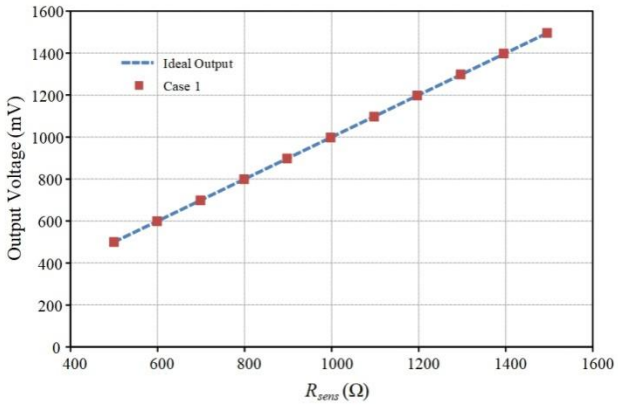


(a)

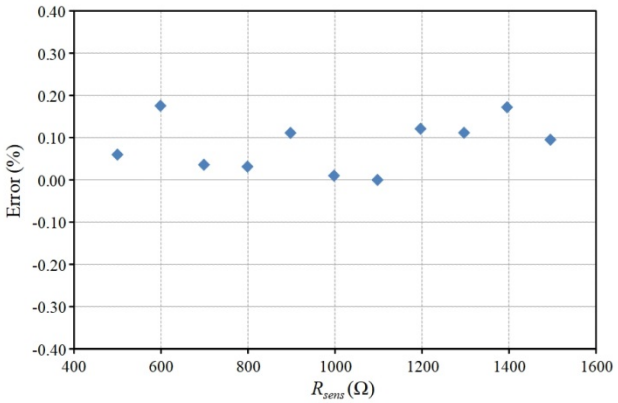


(b)

Fig. 12. The results of case 1 for the sensing resistance $R_{sens}$ in the range of 0.5 kΩ to 1.5 kΩ: (a) plots of the measured output voltage ($V_{out}$) against the sensing resistance ($R_{sens}$) and (b) plots of the error of the proposed circuit against the sensing resistance ($R_{sens}$).

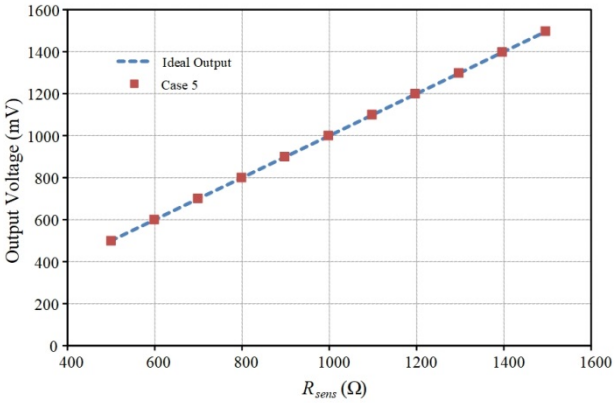


(a)

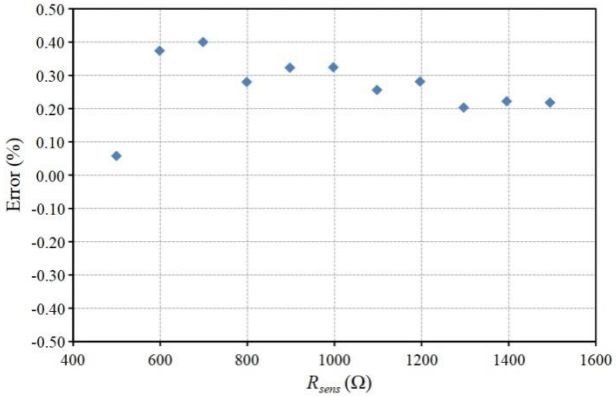


(b)

Fig. 13. The results of case 5 for the sensing resistance $R_{sens}$ in the range of 0.5 kΩ to 1.5 kΩ: (a) plots of the measured output voltage ($V_{out}$) against the sensing resistance ($R_{sens}$) and (b) plots of the error of the proposed circuit against the sensing resistance ($R_{sens}$).

TABLE III: EXPERIMENTAL RESULTS OF THE PROPOSED CIRCUIT OF FIG. 8 FOR DIFFERENT VALUES OF LEAD-WIRE RESISTANCES

| $R_{sens}$ (Ω) | Calculated $V_o$ (mV) | Measured $V_o$ (mV) | | | | | Worst-case error (%) |
|---|---|---|---|---|---|---|---|
| | | Case 1 | Case 2 | Case 3 | Case 4 | Case 5 | |
| 499.5 | 499.5 | 499.80 | 500.80 | 500.04 | 499.69 | 499.79 | 0.2603 |
| 598.5 | 598.5 | 599.55 | 600.45 | 599.80 | 600.36 | 600.74 | 0.3743 |
| 698.5 | 698.5 | 698.75 | 701.15 | 699.49 | 700.77 | 701.30 | 0.4001 |
| 798.5 | 798.5 | 798.75 | 800.55 | 799.44 | 800.55 | 800.74 | 0.2799 |
| 897.5 | 897.5 | 898.50 | 901.30 | 898.91 | 900.57 | 900.40 | 0.4234 |
| 997.5 | 997.5 | 997.60 | 1000.50 | 999.00 | 1000.56 | 1000.74 | 0.3243 |
| 1097.5 | 1097.5 | 1097.50 | 1096.46 | 1098.26 | 1100.01 | 1100.31 | 0.2560 |
| 1196.5 | 1196.5 | 1197.95 | 1196.75 | 1197.79 | 1199.75 | 1199.87 | 0.2817 |
| 1296.5 | 1296.5 | 1297.95 | 1297.55 | 1297.24 | 1300.16 | 1299.14 | 0.2819 |
| 1395.5 | 1395.5 | 1397.90 | 1396.70 | 1396.69 | 1398.55 | 1398.60 | 0.2221 |
| 1495 | 1495 | 1496.43 | 1493.73 | 1496.32 | 1498.65 | 1498.26 | 0.2441 |

Fig. 12 illustrates the results of case 1 for the sensing resistance $R_{sens}$ varied from 0.5 kΩ to 1.5 kΩ. Fig. 12(a) and (b) shows the plots of the measured output voltage ($V_{out}$) and the errors of the proposed circuit against the sensing resistance $R_{sens}$, respectively. The results of case 5 for the sensing resistance $R_{sens}$ varied from 0.5 kΩ to 1.5 kΩ are shown in Fig. 13. The plots of the measured output voltage ($V_{out}$) and the errors of the proposed circuit against the sensing resistance $R_{sens}$ are demonstrated in Fig. 13 (a) and (b), respectively.

From Fig. 12 and Fig. 13, it can be seen that the proposed interfacing circuit can produce the voltage output corresponding to the sensing resistance $R_{sens}$ with good linearity. The maximum errors of cases 1 and 5 are about 0.1754% and 0.4001%, respectively. The measured output voltage ($V_{out}$) of the proposed interfacing circuit is shown in Table III. From Table III, the maximum error of 5 experimental cases is about 0.4234%.

## VI. ERRORS OF THE PROPOSED CIRCUIT

The output voltage of the proposed circuit can be defined by Eq. (9). However, the voltage drop of each diode is practically mismatched. If $V_{D2} = V_{D1} \pm \Delta V_D$ is defined, the Eq. (8) can be written as

$$V_{out} = 0.5\left( R_{sens} \frac{V_{ex}}{R_X} + V_{D1} - \left(V_{D1} \pm \Delta V_D\right) \right) \quad (10)$$

where $\Delta V_D$ is the mismatched voltage of $D_1$ and $D_2$. From Eq. (10), the error from the mismatch of the voltage drop of diodes can be expressed as

$$\text{Error} = \frac{\left\{\left(0.5R_{\text{sens}}\frac{V_{\text{ex}}}{R_X}\right)-\left(0.5\left(R_{\text{sens}}\frac{V_{\text{ex}}}{R_X}+V_{D1}-\left(V_{D1}\pm\Delta V_D\right)\right)\right)\right\}}{0.5R_{\text{sens}}\frac{V_{\text{ex}}}{R_X}}$$

$$= \frac{\pm\Delta V_D R_X}{R_{\text{sens}}V_{\text{ex}}} \quad (11)$$

From Eq. (11), the error is caused by the mismatch of the voltage drop of diodes used for compensating lead-wire resistance. This means that if the values of $R_X$, $R_{\text{sens}}$ and $V_{\text{ex}}$ are fixed, the error in the output voltage of the proposed circuit depends on the difference in the voltage drop of each diode for compensating lead-wire resistance. If the difference of the voltage drop of each diode equals zero (matched diode), the error will be zero.

## VII. Conclusions

A simple technique for circuit design to compensate for the effects of lead-wire resistance has been described in this paper. The proposed interfacing circuit is used for compensating the lead-wire resistance with voltage output corresponding to the sensor resistance. The proposed circuit consists of a square wave generator, a Current Feedback Operational Amplifier (CFOA), a Sallen-key low-pass filter, and opamps. The opamp is placed to the input of CFOA to reduce the effect of the internal resistance of port x and improve the accuracy of the proposed circuit. The simulation studies show that the improved interfacing circuit can compensate for the effect of lead-wire resistance and increase the accuracy of the proposed circuit. The experimental results of the improved interfacing circuit show that the proposed circuit can compensate for the effect of lead-wire resistance and increase the accuracy of the output voltage with a maximum error of about 0.4234%.

## Conflict of Interest

The authors declare no conflict of interest.

## Author Contributions

Writing–review and editing, Wandee Petchmaneelumka; Circuit simulation and testing, Writing–original draft, Apinai Rerkratn; Circuit implementation and testing, Sirichai Tammaruckwattana; Conceptualization, Anucha Kaewpoonsuk; All authors have read and agreed to the published version of the manuscript.

## References


[1] S. Nihtianov and A. Luque, *Smart Sensors and MEMs*, 2nd ed., Woodhead Publishing, 2018, pp. 171–219.

[2] W. Y. Du, *Resistive, Capacitive, Inductive, and Magnetic Sensor Technologies*, 1st ed., CRC Press, 2014.

[3] W. Y. Du, Resistive, *Capacitive, Inductive, and Magnetic Sensor Technologies*, United Kingdom: Taylor & Francis, 2014.

[4] S. Das, M. Bhattacharjee, K. Thiyagarajan, and S. Kodagoda, "Nonlinear response analysis of a polymer-based piezoresistive flexible tactile sensor at low pressure," *IEEE Sensors Letters*, vol. 7, no. 11, pp. 1–4, Nov. 2023.

[5] J. Zikulnig, L. Neumaier, M. Lenzhofer, S. Carrara, and J. Kosel, "Laser-induced graphene on chitosan: An enabling technology for sustainable resistive humidity sensors," *IEEE Sensors Letters*, vol. 7, no. 9, pp. 1–4, Sept. 2023.

[6] Y. Shen, H. Li, E. Cantatore, and P. Harpe, "A dynamic resistive temperature sensor with fully integrated corrections," *IEEE Solid-State Circuits Letters*, vol. 6, pp. 173–176, 2023.

[7] P. Fang, Y. Zhu, W. Lu *et al.*, "Smart glove human-machine interface based on strain sensors array for control UAV," *International Journal of Electrical and Electronic Engineering & Telecommunications*, vol. 12, no. 3, pp. 216–222, May 2023.

[8] J. Wagner, H. Winger, C. Cherif, and F. Ellinger, "Smart glove with fully integrated textile sensors and wireless sensor frontend for the tactile internet," *IEEE Sensors Letters*, vol. 7, no. 2, pp. 1–4, Feb. 2023.

[9] W. Dong, L. Yang, and G. Fortino, "Stretchable human machine interface based on smart glove embedded with PDMS-CB strain sensors," *IEEE Sensors Journal*, vol. 20, no. 14, pp. 8073–8081, 2020.

[10] Y. Zhu, Z. Ding, F. Zhang *et al.*, "New pulse recognition system for coronary heart disease patients based on pressure sensors," *International Journal of Electrical and Electronic Engineering & Telecommunications*, vol. 12, no. 4, pp. 288–293, July 2023.

[11] M. Zafar and B. Wei, "Comparison analysis of thermistor and RTD for energy transfer station application," in *Proc.* 2023 *IEEE/ASME International Conference on Advanced Intelligent Mechatronics (AIM), Seattle*, WA, USA, 2023, pp. 800–805.

[12] K. Elangovan and A. C. Sreekantan, "Metrological evaluation of robust relaxation-oscillator interface for remote resistive sensors and its application toward realizing few industrial measurement systems," *IEEE Open Journal of Instrumentation and Measurement*, vol. 2, pp. 1–9, 2023.

[13] M. Pandya, B. Bhaisare, A. Datir, K. Ghadole, A. Gupta, and D. Rotake, "Resistive readout circuit for chemiresistive sensor interfacing with android application," presented at 2023 4th International Conference for Emerging Technology, Belgaum, India, 2023.

[14] A. Depari, P. Bellagente, P. Ferrari *et al*., "Versatile and low-cost sensor interface for IoT-ready odor monitoring in wastewater management," in *Proc. 2021 IEEE Sensors Applications Symposium*, Sundsvall, 2021, pp. 1–6.

[15] F. Reverter, "A front-end circuit for two-wire connected resistive sensors with a wire-resistance compensation," *Sensors*, vol. 23, no. 19, #8228, 2023.

[16] A. Rerkratn, S. Prombut, T. Kamsri *et al.*, "A procedure for precise determination and compensation of lead-wire resistance of a two-wire resistance temperature detector," *Sensors*, vol. 22, #4176, 2022.

[17] W. Li, S. Xiong, and X. Zhou, "Lead-wire-resistance compensation technique using a single Zener diode for two-wire resistance temperature detectors (RTDs)," *Sensors*, vol. 20, #2742, 2020.

[18] T. Mathew, K. Elangovan, and A. C. Sreekantan, "Accurate interface schemes for resistance thermometers with lead resistance compensation," *IEEE Trans. on Instrumentation and Measurement*, vol. 72, pp. 1–4, 2023.

[19] K. Elangovan and A. C. Sreekantan, "Relaxation Oscillator Based Digital Interface Circuit for Resistive Sensors," in *Proc. 2020 IEEE 17th India Council International Conference*, New Delhi, India, 2020, pp. 1–5.

[20] K. Elangovan and A. C. Sreekantan, "Simple and efficient relaxation-oscillator-based digital techniques for resistive sensors Design and performance evaluation," *IEEE Trans. on Instrumentation and Measurement*, vol. 69, no. 9, pp. 6070–6079, Sept. 2020.

[21] K. Elangovan, S. Dutta, A. Antony, and A. C. Sreekantan, "Performance verification of a digital interface suitable for a broad class of resistive sensors," *IEEE Sensors Journal*, vol. 20, no. 23, pp. 13901–13909, Dec. 2020,

[22] E. Gómez-Ramírez, L. A. Maeda-Nunez, L. C. Álvarez-Simón *et al.* "A highly robust interface circuit for resistive sensors," *Electronics*, vol. 8, 263, 2019.

[23] G. Singh, S. Sohail, U. Mangalanathan, U. Gandhi, and T. Islam, "A novel dual-slope resistance to digital converter with lead resistance compensation," *IEEE Trans. on Instrumentation and Measurement*, vol. 72, pp. 1–10, 2023.
[24] G. Singh, U. Mangalanathan, U. Gandhi, and S. Sohail, "Improved resistance to digital converter for low-value resistive sensor with lead wire compensation," presented at 2022 IEEE Region 10 Symposium (TENSYMP), Mumbai, India, 2022.
[25] K. Elangovan and A. C. Sreekantan, "A simple digitization scheme for resistive sensors and its adaptation for remote measurements," in *Proc. 2021 IEEE International Instrumentation and Measurement Technology Conference*, Glasgow, United Kingdom, 2021, pp. 1–6.
[26] K. Elangovan and A. C. Sreekantan, "Evaluation of new digital signal conditioning techniques for resistive sensors in some practically relevant scenarios," *IEEE Trans. on Instrumentation and Measurement*, vol. 70, pp. 1–9, 2021.
[27] T. Sen, A. C. Sreekantan, and S. Sen, "Novel Σ-Δ-based direct digitizers for single-element resistive sensors with considerations on lead-wire compensation," *IEEE Trans. on Instrumentation and Measurement*, vol. 71, pp. 1–10, 2022.
[28] J. A. Hidalgo-López, "Direct interface circuits for resistive sensors affected by lead wire resistances," *Measurement*, vol. 218, pp. 1–7, 2023.
[29] P. R. Nagarajan, B. George, and V. J. Kumar, "Improved single-element resistive sensor-to-microcontroller interface," *IEEE Trans. on Instrumentation and Measurement*, vol. 66, no. 10, pp. 2736–2744, Oct. 2017.
[30] R. Anandanatarajan, U. Mangalanathan, and U. Gandhi, "Enhanced microcontroller interface of resistive sensors through resistance-to-time converter," *IEEE Trans. on Instrumentation and Measurement*, vol. 69, no. 6, pp. 2698–2706, June 2020.
[31] T. K. Maiti, "A novel lead-wire resistance compensation technique using two-wire resistance temperature detector," *IEEE Sensors Journal*, vol. 6, no. 6, pp. 1454–1458, 2006.
[32] T. Kr. Maiti and A. Kar, "Novel remote measurement technique using resistive sensor as grounded load in an opamp based V-to-I converter," *IEEE Sensors Journal*, vol. 9, no. 3, pp. 244–245, 2009.
[33] W. Petchmaneelumka, P. Julsereewong, A. Julsereewong, and J. Tongpakpanang, "Simple interface circuit with lead-wire-resistance compensation for single resistive sensors," in *Proc. 2012 12th Int. Conf. on Control, Automation and Systems*, Jeju, Korea, 2012, pp. 1076–1079.
[34] E. Ebrahimi and S. Naseh, "A colpitts CMOS quadrature VCO using direct connection of substrates for coupling," *IEEE Trans. on Very Large Scale Integration (VLSI) Systems*, vol. 21, no. 3, pp. 571–574, 2013.
[35] Y. Majd and E. Ebrahimi, "Analysis and design of a new low-phase noise and Gm-enhanced class-C quadrature VCO," *IET Microw Antennas Propag*, vol. 14, no. 13, pp. 1537–1546, 2020.
[36] S. G. Gift, "Hybrid current conveyor operational amplifier circuit," *International Journal of Electronics*, vol. 88, no. 12, pp. 1225–1235, Dec. 2001.
[37] A. Julsereewong, P. Julsereewong, T. Rungkhum, and H. Sasaki, "Interface circuit using operational conveyors for differential resistive sensors," in *Proc. 10th Int. Conf. on Electrical Engineering/Electronics, Computer, Telecommunications and Information Technology*, Krabi, Thailand, 2013. doi: 10.1109/ECTICon.2013.6559501



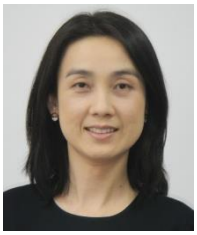

**Wandee Petchmaneelumka** was born in Rayong, Thailand. She received the D.Eng. degree in electrical engineering from the King Mongkut's Institute of Technology Ladkrabang (KMITL), Bangkok, Thailand, in 2009. He is currently an associate professor at the Department of Instrumentation and Control Engineering, School of Engineering, King Mongkut's Institute of Technology Ladkrabang (KMITL). Her research interests include Fieldbus communication network, signal processing, instrumentation and measurement systems, and system dynamics and modeling.

**Apinai Rerkratn** was born in Suphanburi, Thailand, on August 26, 1974. He received the B.Eng. degree in telecommunication engineering, and the M.Eng. and the D.Eng. degrees in electrical engineering from the King Mongkut's Institute of Technology Ladkrabang (KMITL), Bangkok, Thailand, in 1998, 2002, and 2013, respectively. Since 2014, He is currently an associate professor at the Department of Instrumentation and Control Engineering, School of Engineering, King Mongkut's Institute of Technology Ladkrabang (KMITL). His research interests are in the areas of analog circuit design for electronic instrumentation, signal and image processing, and wireless sensor network.

**Sirichai Tammaruckwattana** received the B.E. and M.E. degrees in electrical and control engineering from King Mongkut's Institute of Technology Ladkrabang, Bangkok, Thailand and D.Eng. degree in material science and production engineering from Fukuoka Institute of Technology, Fukuoka, Japan, in 2001, 2005, and 2015, respectively. In December 2005, he joined the Department of Instrumentation and Control Engineering, King Mongkut's Institute of Technology Ladkrabang, Bangkok, Thailand, as a Lecturer. In November 2016, he is currently assistant professor in the department. His current research interests include wind power generation system.

**Anucha Kaewpoonsuk** was born in Phitsanulok, Thailand in 1974. He received the B.Sc. degree in physics-computer and electronics from Naresuan University, Phitsanulok, Thailand, in 1997 and the M. Eng. and D. Eng. degree in electrical engineering from the King Mongkut's Institute of Technology Ladkrabang (KMITL), Bangkok, Thailand, in 2001 and 2008, respectively. He is currently an associate professor at the Department of Physics, Naresuan University. His research interests include electronic instrumentation, measurement system, analog and digital circuit designs.